



Cross-comparison of systemic and tissue-specific metabolomes in a mouse model of Leigh syndrome

Karin Terburgh¹ · Jeremie Z. Lindeque¹ · Francois H. van der Westhuizen¹ · Roan Louw¹

Received: 20 August 2021 / Accepted: 3 November 2021 / Published online: 18 November 2021
© The Author(s), under exclusive licence to Springer Science+Business Media, LLC, part of Springer Nature 2021

Abstract

Introduction The value of metabolomics in multi-systemic mitochondrial disease research has been increasingly recognized, with the ability to investigate a variety of biofluids and tissues considered a particular advantage. Although minimally invasive biofluids are the generally favored sample type, it remains unknown whether systemic metabolomes provide a clear reflection of tissue-specific metabolic alterations.

Objectives Here we cross-compare urine and tissue-specific metabolomes in the *Ndufs4* knockout mouse model of Leigh syndrome—a complex neurometabolic MD defined by progressive focal lesions in specific brain regions—to identify and evaluate the extent of common and unique metabolic alterations on a systemic and brain regional level.

Methods Untargeted and semi-targeted multi-platform metabolomics were performed on urine, four brain regions, and two muscle types of *Ndufs4* KO ($n \geq 19$) vs wildtype ($n \geq 20$) mice.

Results Widespread alterations were evident in alanine, aspartate, glutamate, and arginine metabolism in *Ndufs4* KO mice; while brain-region specific metabolic signatures include the accumulation of branched-chain amino acids, proline, and glycolytic intermediates. Furthermore, we describe a systemic dysregulation in one-carbon metabolism and the tricarboxylic acid cycle, which was not clearly reflected in the *Ndufs4* KO brain.

Conclusion Our results confirm the value of urinary metabolomics when evaluating MD-associated metabolites, while cautioning against mechanistic studies relying solely on systemic biofluids.

Keywords *Ndufs4* knockout mice · Brain regions · Metabolomics · Mitochondrial disease · Complex I deficiency · Leigh syndrome

Abbreviations

1C	One-carbon	FDR	False discovery rate
3-MH	3-methylhistidine	G3P	Glycerol-3-phosphate
BCAA	Branched-chain amino acids	GC-TOF-MS	Gas chromatography time-of-flight mass spectrometry
BBD	γ -butyrobetaine dioxygenase	GLUT1	Glucose transporter 1
BHMT	Betaine-homocysteine methyltransferase	HP	Hydroxyphenyl
CI	Complex I	KO	Knockout
CII	Complex II	LC-MS/MS	Liquid chromatography-tandem mass spectrometry
CoA	Coenzyme A	LS	Leigh syndrome
DHAP	Dihydroxyacetone phosphate	MD	Mitochondrial disease
ES	Effect size	NAD(P)H	Nicotinamide adenine dinucleotide (phosphate)
ETFDH	Electron-transferring-flavoprotein dehydrogenase	NAG	N-acetyl glutamate
		OXPHOS	Oxidative phosphorylation
		P	Postnatal day
		Q	Ubiquinone
		SAM	S-adenosyl methionine
		SCF	Short chain fatty acids

✉ Roan Louw
Roan.Louw@nwu.ac.za

¹ Human Metabolomics, Faculty of Natural and Agricultural Sciences, North-West University (Potchefstroom Campus), Private Bag X6001, Potchefstroom, South Africa

TCA	Tricarboxylic acid
WT	Wild type

1 Introduction

A clear understanding of the pathologies and treatment of primary mitochondrial diseases (MDs), which results from a dysfunction of the oxidative phosphorylation (OXPHOS) system, remain a great challenge. Largely unknown mechanisms govern a tissue-specific vulnerability to MD-causing mutations and an extreme heterogeneity in genotype-phenotype correlations among patients (Lake et al., 2016; Mootha and Chinnery, 2018; Rahman, 2020). As the most common form of MD, respiratory chain complex I (CI) deficiency and its most prevalent pediatric manifestation, Leigh syndrome (LS, OMIM # 256000), are at the forefront of MD research (Rahman et al., 1996; Rodenburg, 2016). The *Ndufs4* knockout (KO) mouse model of LS suffers from all-pervading CI deficiency, exhibits progressive focal lesions in specific brain regions, and displays symptoms similar to human patients. Symptoms include developmental delay, failure to thrive, locomotor impairment, encephalomyopathy and respiratory deficits, which progressively worsen until premature death (Kruse et al., 2008; Quintana et al., 2010). Studies on *Ndufs4* KO mice have revealed that specific neuronal populations (linked to lesion-prone brain regions) drive most symptoms (Bolea et al., 2019), while peripheral tissues, like skeletal muscle, seem relatively unaffected phenotypically (Alam et al., 2015; Chouchani et al., 2014; Kruse et al., 2008). However, the contribution of systemic metabolic alterations to this neurometabolic disease cannot be ruled out (Bolea et al., 2019; Di Meo et al., 2017; Ito et al., 2017; Lee et al., 2019).

Metabolomics present a powerful tool with which to analyze the downstream effects of multi-systemic diseases like MD in a holistic manner (Rahman and Rahman, 2018). Although the application of metabolomics in the field of MD research is relatively novel, it has made significant progress in recent years—especially with the increased availability of well characterized MD models (Esterhuizen et al., 2017). Non-invasive (urine) or minimally invasive (blood) systemic samples are generally favored for metabolomics investigations of MD. However, it remains inconclusive whether such samples are optimal to study and/or monitor MD, and how well systemic metabolomes reflect tissue-specific metabolic alterations (Esterhuizen et al., 2017; Steele et al., 2017). A few metabolomics studies have been performed on *Ndufs4* KO tissues (Emmerzaal et al., 2020; Jin et al., 2014; Johnson et al., 2020; Johnson et al., 2013; Terburgh et al., 2021a; Terburgh et al., 2019b), however, the link between systemic and brain regional metabolomes remains unexplored. Here, we integrate and cross-compare tissue and urine metabolomes

from *Ndufs4* KO vs wildtype (WT) mice to establish whether differences exist between brain region-specific and systemic metabolic profiles in LS. Skeletal muscle metabolomes were included in this comparison to show the contribution of peripheral tissues. Seven sample types from individual late stage diseased *Ndufs4* KO and WT mice were extensively investigated via untargeted and semi-targeted multiplatform metabolomics. These samples include one lesion-resistant brain region (anterior cortex); three lesion-prone brain regions (brainstem, cerebellum, and olfactory bulbs); urine collected overnight; the primarily glycolytic white parts of the quadriceps femoris; and the primarily oxidative solei.

2 Materials and methods

2.1 Animals and housing

Male whole-body homozygous *Ndufs4* KO mice, along with age- and sex-matched controls (WT) were used. Only one sex-group was used in order to minimize sex-related metabolic variation due to known differences in hormone cycles, tissue-specific metabolism and metabolic profiles between sexes (Ruoppolo et al., 2018; Wells et al., 2016; Wu and Gao, 2015). KO mice were born from heterozygous crosses (B6.129S4-*Ndufs4*^{tm1.1Rpa}/J) obtained from Jackson Laboratory (JAX stock #027058). *Ndufs4* genotypes were confirmed by polymerase chain reaction using tail snips. The animals were bred and housed at the specific pathogen-free unit of the Vivarium (SAVC reg. no. FR15/13458) of the Pre-Clinical Drug Development Platform (PCDDP; NWU, RSA) and approval (NWU-00378-16-A5) for this study was obtained from the Animal Research Ethics Committee of the NWU. Animals were group housed under temperature- ($22 \pm 1^\circ\text{C}$), humidity- ($55 \pm 10\%$) and light-controlled (12:12 hour light/dark cycle) conditions with standard laboratory chow (Rodent Breeder, #RM1845, LabChef, Nutritionhub) and water provided *ad libitum*. Samples were collected between P45-50 as this age range was selected to represent the late stage of LS, based on our previous survival curves and phenotypic analyses (Miller et al., 2021).

2.2 Sample collection

Urine was collected from individual mice in metabolic cages after overnight (12 hours) fasting with *ad libitum* access to water. Since *Ndufs4* KO mice yielded limited urine volumes, urine droplets that failed to reach the collection tube were also collected. Hence, the separating cone, collection funnel and -tubes were all treated with sodium azide (NaN_3 ; 0.1% (w/v); WT: 100 μL and KO: 50 μL) to prevent bacterial growth. After urine collection, mice were euthanized via cervical dislocation at the same time of day (8:00-9:00

AM). The brain was immediately removed from the skull, rinsed with saline solution (SABAX PBS; 0.9% NaCl (w/v), #7634, Adcock Ingram) and dissected into the regions of interest (anterior cortex, brainstem, cerebellum, and olfactory bulbs). Concurrently, the white muscle portions of quadriceps femoris, as well as solei muscles, were collected from both hind limbs. All samples were snap frozen in liquid nitrogen upon collection (within 15 min post-mortem for tissues) and stored at -80°C until use.

2.3 Metabolic profiling

2.3.1 Sample analysis

Untargeted gas chromatography time-of-flight mass spectrometry (GC-TOF-MS) and semi-targeted liquid chromatography-tandem mass spectrometry (LC-MS/MS) were performed on seven sample types from *Ndufs4* KO ($n \geq 19$) and WT ($n \geq 20$) mice. Tissue extracts were individually prepared and analyzed as previously described (Terburgh et al., 2021a; Terburgh et al., 2019b), while detailed descriptions on urine sample preparation and analysis are given in the supplementary information. In short, frozen tissues were weighed and homogenized in the presence of internal standards added according to tissue mass. Monophasic tissue extracts were prepared via modified Bligh-Dyer (Gullberg et al., 2004) (methanol/water/chloroform, 3:1:1), with additional step-wise extraction (Wu et al., 2008) to obtain polar phases of biphasic brain extracts (methanol/water/chloroform, 2:1.8:2) for LC-MS/MS. Tissue extracts were divided between the platforms, with stable isotopes added to LC-MS/MS samples. Pre-determined volumes of urine, containing 0.0625 μmole creatinine, were supplemented with internal standards (included stable isotopes for LC-MS/MS samples) and deproteinized using methanol. Urine and tissue extracts were then dried under nitrogen and derivatized prior to their analysis. For GC-TOF-MS, samples were oximated and silylated, while LC-MS/MS samples were butylated.

2.3.2 Data processing

Spectral data matrices were individually inspected (correct peak detection and alignment, batch precision and data integrity) and preprocessed (data filtering, half-minimum missing value imputation and normalization). Tissue data was normalized post-acquisition to tissue mass (ng/mg tissue) using internal standards, 3-phenylbutyric acid (GC-TOF-MS) and *N, N*-dimethylphenylalanine (LC-MS/MS). Additionally, LC-MS/MS metabolites were also normalized to isotope internal standards to account for ion suppression effects. Urine data was normalized pre-acquisition to creatinine content (mg/g creatinine) and post-acquisition to tropic acid (GC-TOF-MS) or isotope (LC-MS/MS) internal

standards. Metabolites detected via LC-MS/MS were normalized to their own isotopes, where available, or an isotope with a similar retention time to which the metabolite strongly correlated in QC samples. Finally, the data was log transformed and outliers were detected (PCA Hotelling's T^2 ellipses, loadings plot and biplots). Data processing was done using Excel (Microsoft 365), Statistica v 13.0 (TIBCO Software Inc.) and MetaboAnalyst v 4.0 (Xia Lab (Chong et al., 2018)). The metabolomics data obtained in this study can be accessed at the Common Fund's National Metabolomics Data Repository (NMDR) website, the Metabolomics Workbench (<https://www.metabolomicsworkbench.org>) where it has been assigned project IDs: PR000721 (Terburgh et al., 2019a), PR001003 (Terburgh et al., 2021b), and PR001187 (Terburgh et al., 2021c).

2.3.3 Statistical analyses

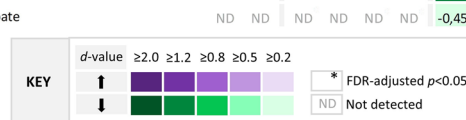
For each sample type, univariate analyses were used to determine discriminatory features between *Ndufs4* KO and WT metabolic profiles. Statistical and practical significance were determined using the student's t-test and effect size (ES, Cohen's d -value) calculations, respectively. False discovery rate (FDR) corrected p -values were calculated in MetaboAnalyst (Chong et al., 2018), with an FDR- p of ≤ 0.05 considered statistically significant. Dataset features were identified via spectral and retention time matching using commercial and in-house spectral libraries together with public databases. Metabolite identities were assigned to spectral features with high confidence levels (Table S2) ranging from level one to three, as defined by Schymanski et al. (2014). For each sample type, pathway analysis was performed on significantly altered metabolites using MetaboAnalyst (Chong et al., 2018). Compound labels were matched to HMDB and KEGG IDs, with *mus musculus* (mouse) KEGG as the selected pathway library. Hypergeometric test was the selected over-representation analysis method for pathway enrichment analysis, while relative betweenness centrality was the selected node importance measure for pathway topology analysis.

3 Results and discussion

3.1 Cross-comparison of urine- and tissue metabolomes

Several significant metabolic alterations were observed in the urine and tissue-specific metabolomes of *Ndufs4* KO vs WT mice, with the number of discriminatory metabolites (and their significance level) generally lower in the muscles. Figure 1A–J illustrates the main similarities and differences among the metabolic alterations seen in the seven

		WQ	SOL	AC	BS	CB	OB	U
A	Aspartate & glutamate metabolism							
LC	Glutamine	-0.61	-0.10	0.00	0.33	-0.14	-0.49	-2.40
LC	Glutamate	-0.58	-0.32	-1.78	-1.09	-1.13	-1.26	-1.35
GC	Pyroglutamate	-0.56	-0.12	-0.94	-1.53	-1.71	-0.72	-0.96
LC	3-Aminobutyrate (GABA)	-0.23	0.45	-0.24	-0.27	-0.42	-0.48	-2.09
LC	Aspartate	-0.31	0.03	-2.33	-1.21	-1.58	-1.72	-0.51
LC	Asparagine	0.80	0.72	-1.81	-1.63	-1.80	-1.05	-0.49
LC	N-acetylglutamate	-0.75	0.08	0.94	1.22	0.78	0.17	-2.86
LC	N-acetylaspartate	1.63	0.99	-0.03	-0.27	-0.19	1.03	ND
B	Arginine & proline metabolism							
GC	Carbamate	ND	ND	0.82	-0.08	-0.22	0.65	-0.95
LC	Ornithine	0.27	0.78	-0.82	-1.01	-0.26	-0.14	-0.73
LC	Citrulline	-1.04	-0.56	-1.26	-1.66	-0.72	-0.27	-1.00
LC	Arginine	0.37	0.68	-1.66	-0.03	-1.18	1.37	-1.34
GC	Urea	0.28	0.69	0.20	0.40	0.33	0.26	0.09
GC	Putrescine	ND	ND	1.23	1.35	0.53	2.69	ND
LC	Proline	-1.80	-0.40	0.79	2.75	2.38	1.59	-1.94
LC	Hydroxyproline	-1.32	-1.04	-1.65	-1.44	-1.75	-0.73	-3.02
LC	Creatine	0.28	0.40	0.68	-0.05	-0.07	0.31	-0.62
GC	Creatinine	-2.15	-1.60	-0.76	-0.23	-0.48	-0.03	ND
C	Lysine & tryptophan metabolism							
LC	Lysine	0.83	1.25	0.08	-0.16	0.15	2.43	-0.57
LC	Carnitine (C0)	-0.68	-0.10	0.66	0.46	0.53	1.41	0.67
LC	Pipecolate	1.13	1.56	0.99	1.02	0.46	1.75	ND
LC	5-Hydroxylysine	ND	ND	ND	ND	ND	ND	-0.64
LC	2-Aminoadipate	-1.88	-1.47	-1.66	-1.54	-1.90	-3.22	-0.98
GC	2-Hydroxyadipate	ND	ND	ND	ND	ND	ND	-2.75
LC	Tryptophan	-0.34	-0.01	0.01	-0.01	0.25	0.61	-0.56
LC	Kynurenone	ND	ND	ND	ND	ND	ND	-0.57
GC	5-Hydroxy-indole	ND	ND	ND	ND	ND	ND	-1.44
GC	Glutarate	ND	ND	ND	ND	ND	ND	-1.26
D	Histidine metabolism							
LC	Histidine	0.34	1.01	0.16	0.41	-0.16	0.34	1.11
LC	3-Methylhistidine	0.83	1.14	0.75	1.40	0.51	1.01	-1.17
LC	1-Methylhistidine	-0.73	-0.34	-0.06	-0.29	0.55	-0.11	-1.10
E	Lipid metabolism							
GC	Glycerol	-0.8	* -0.7	0.56	0.86	-0.29	-1.16	-1.27
GC	Palmitate (C16:0)	-0.60	-0.49	0.38	0.33	0.36	1.06	ND
GC	Stearate (C18:0)	-0.30	-0.09	0.12	0.16	0.00	-0.89	ND
GC	Oleate (C18:1)	-0.29	-0.31	0.46	0.68	0.77	1.44	ND
GC	Arachidonate (C20:4, ω-6)	ND	ND	0.82	0.59	0.70	0.73	ND
GC	25-Hydroxycholesterol	ND	ND	-0.22	-1.47	-0.75	-0.68	ND
GC	9S,10S-Dihydroxystearate	ND	ND	-0.83	-0.65	0.49	-0.56	ND
LC	Acetylcarnitine (C2)	1.03	0.04	0.54	0.55	0.18	0.93	0.55
LC	Propionylcarnitine (C3)	-0.44	-0.78	-0.45	-1.22	-1.39	0.36	1.35
LC	Butyrylcarnitine (C4)	-1.34	0.99	-0.45	-1.09	-1.61	-0.93	-0.11
GC	Butyrylglycine (C4)	ND	ND	ND	ND	ND	ND	-1.58
GC	Valerylglycine (C5)	ND	ND	ND	ND	ND	ND	-1.94
LC	Hexanoylcarnitine (C6)	-0.94	-0.46	ND	ND	ND	-0.63	-0.48
GC	Hexanoylglycine (C6)	ND	ND	ND	ND	ND	ND	-1.42
LC	Octanoylcarnitine (C8)	-0.99	-0.06	0.08	0.21	0.11	-0.04	-1.12
LC	Decanoylcarnitine (C10)	ND	ND	ND	ND	ND	ND	-0.97
GC	Malonate	ND	ND	0.05	-0.19	-0.33	0.81	0.34
GC	Hydroxymalonate (Tartronate)	ND	ND	ND	ND	ND	ND	-1.50
F	TCA cycle metabolism							
GC	2-Ketoglutamate	ND	ND	ND	ND	0.20	0.87	
GC	2-Hydroxyglutarate	-0.17	-1.40	-1.59	-1.59	-0.79	-1.10	-1.09
GC	Succinate	-0.92	-0.40	-0.75	-0.85	-0.78	-0.79	-0.60
GC	Fumarate	-0.51	-0.64	-0.24	0.02	0.14	0.01	1.71
GC	Malate	-0.91	-1.01	0.04	0.29	0.43	0.34	1.40
GC	Citramalate	ND	ND	ND	ND	ND	ND	1.79
G	BCAA metabolism							
LC	Valine	0.24	0.36	0.94	1.73	2.15	1.51	-1.47
LC	Isoleucine-leucine	-0.12	0.31	0.75	1.65	1.91	1.63	-2.13
GC	Isoleucine	-0.28	0.33	0.62	1.50	1.43	1.54	ND
GC	Leucine	0.16	0.29	0.43	1.33	2.07	1.66	ND
LC	Isovalerylcarnitine (C5)	-0.62	* -0.97	-0.64	1.90	2.73	-1.36	0.03
GC	Isovalerylglycine (C5)	ND	ND	ND	ND	ND	ND	1.20
GC	Methylsuccinate	ND	ND	ND	ND	ND	ND	0.76
GC	3-Hydroxymethylglutarate	ND	ND	ND	ND	ND	ND	-0.66
H	One-carbon metabolism							
LC	Glycine	0.06	0.37	-0.43	0.81	-0.87	0.10	-1.10
LC	Methionine	-0.78	0.01	-0.39	-0.13	-0.49	0.01	-1.71
LC	Trimethylglycine (betaine)	-0.61	0.24	-0.47	-0.23	-0.70	0.09	-2.53
LC	Dimethylglycine	-2.49	-2.45	ND	ND	ND	ND	-2.78
LC	Methylglycine (sarcosine)	-0.80	-0.36	ND	ND	ND	ND	-3.33
LC	Threonine	-0.92	0.17	0.02	0.38	-0.06	0.60	-1.06
LC	Serine	-0.04	0.65	-1.04	-2.07	-1.34	0.26	-1.51
LC	Cystathione	0.73	-0.40	0.45	0.22	0.58	1.70	-1.53
GC	Cysteine	ND	ND	-1.19	0.32	-0.17	-0.01	ND
LC	Cystine	ND	ND	-0.31	0.08	ND	ND	-0.82
GC	Formylglycine	ND	ND	0.78	0.08	-0.01	1.22	ND
LC	Taurine	0.37	-0.30	0.36	1.26	0.55	0.15	ND
LC	Phenylalanine	-0.32	0.24	-0.10	0.23	-0.22	0.39	-1.20
LC	Isothreonine	ND	ND	0.23	0.06	-0.85	0.17	-0.69
GC	Glycolate	-1.13	ND	-1.25	0.89	-0.66	0.01	ND
GC	Glycerate	-0.79	0.28	ND	ND	ND	ND	-1.00
I	Pyrimidine & purine metabolism							
GC	Orotate	ND	ND	ND	ND	ND	ND	-1.52
GC	UMP	ND	ND	-0.99	-0.42	ND	0.62	ND
GC	Uracil	ND	ND	-0.10	-0.42	-0.43	0.07	-1.71
GC	3-Ureidopropionate	ND	ND	ND	ND	ND	ND	-0.99
LC	Beta-alanine	-0.51	-0.32	-0.15	0.37	-0.40	0.91	-1.32
GC	Pantothenate (vitamin B5)	ND	ND	0.34	0.18	-0.14	0.89	ND
LC	3-Aminoisobutyrate (BAIBA)	ND	0.33	ND	ND	ND	ND	-1.27
GC	Adenosine	ND	ND	-0.15	-0.19	ND	0.94	ND
GC	Urate	ND	ND	ND	ND	ND	ND	-0.83
J	Glycolysis & sugar derivatives							
GC	Glucose	-0.50	-0.54	0.24	0.06	0.60	2.45	-0.78
GC	Glucose-1-phosphate	ND	ND	0.71	ND	2.79	ND	
GC	Glucose-6-phosphate	ND	ND	ND	ND	8.48	ND	
GC	Fructose-6-phosphate	ND	ND	0.54	0.81	ND	3.82	ND
GC	Dihydroxyacetone phosphate (DHAP)	ND	ND	1.22	0.65	0.20	5.19	ND
GC	Glycerol-3-phosphate (G3P)	ND	ND	-2.11	-1.89	-1.43	-0.92	-1.06
GC	Pyruvate	-0.51	-0.54	0.60	0.35	0.66	1.31	1.40
GC	Lactate	-0.52	-0.50	0.01	0.62	0.89	1.48	1.34
LC	Alanine	-0.87	-0.52	0.63	0.55	1.25	1.35	1.00
GC	Ribitol	ND	ND	0.79	1.32	1.37	0.92	-0.84
GC	Ribose	ND	ND	0.16	0.13	ND	ND	-0.99
GC	Ribonate	ND	ND	ND	ND	ND	ND	-2.95
GC	Sorbose	ND	ND	ND	ND	ND	ND	-1.28
GC	Erythro	ND	ND	-1.24	-0.31	-0.99	-0.37	-2.69
GC	Erythronate	ND	ND	1.50	ND	2.13	1.26	ND
GC	Threose	ND	ND	0.80	0.90	-0.28	-1.20	ND
GC	Threonate	ND	ND	ND	ND	ND	ND	-3.45
GC	Mannionate	ND	ND	0.05	0.45	-0.55	1.23	0.21
GC	Oxalate	-0.23	0.51	0.73	-0.29	0.25	0.24	-1.72
GC	Glucurate	ND	ND	ND	ND	ND	ND	-0.87
GC	Gulonate	ND	ND	ND	ND	ND	ND	-1.62
GC	Ascorbate	ND	ND	ND	ND	ND	ND	-0.45



◀Fig. 1 Cross-comparison of metabolic alterations in *Ndufs4* KO mice. Heatmap of effect size (Cohen's *d*) values for each metabolite when relative abundance is compared between *Ndufs4* KO ($n \geq 19$) and WT ($n \geq 20$) mice. Metabolic alterations are compared across seven sample types and grouped according to metabolic pathways (A-J). Shades of purple and green respectively indicate increased and decreased abundance in *Ndufs4* KO mice and correspond to the level of practical significance as indicated in the key. Asterisks indicate statistical significance (FDR-adjusted $p < 0.05$). The first column indicates the analytical platform used for detection. Abbreviations: AC Anterior cortex, BS Brainstem, CB Cerebellum, GC GC-TOF-MS, LC LC-MS/MS, ND Not (reliably) detected, OB Olfactory bulbs, SOL Solei, U Urine, WQ white quadriceps

Ndufs4 KO sample types when compared to their WT counterparts. Reductions in the tissue content and renal excretion of 4-hydroxyproline and 2-amino adipate were among the most significant and consistent alterations observed in *Ndufs4* KO mice compared to WTs (Figs. 2, S1). Furthermore, the levels of citrulline, 2-hydroxyglutarate, succinate, glutamate, pyroglutamate, aspartate, butyrylcarnitine and isovalerylcarnitine also trended lower in most *Ndufs4* KO sample types, with varying levels of significance. The accumulation of branched-chain amino acids (BCAAs), proline, and arachidonate were unique to the four brain regions, although arachidonate could not be detected in other sample types. Additionally, the *Ndufs4* KO urine metabolome contained 51 uniquely altered metabolites (directionality of alterations also considered), many of which could only be detected in urine samples. Combined pathway over-representation and topology analysis (Fig. 3, Table S3) further revealed that alanine, aspartate, and glutamate metabolism were strongly affected (FDR- $p < 0.05$, impact > 0.2) in most *Ndufs4* KO sample types, with the significance level again relatively lower in the muscles. *Ndufs4* KO brain regions and urine further displayed significantly enriched arginine, proline, and BCAA metabolism. Although lesion-resistant and -prone brain regions display generally similar metabolic alterations in *Ndufs4* KO vs WT mice, the practical and statistical significance level of these alterations vary. In our previous work (Terburgh et al., 2021a) we report a graded reduction in CI activity in *Ndufs4* KO brain regions, with the lesion resistant anterior cortex displaying the highest level of residual CI activity and the olfactory bulbs displaying the lowest [AC (38% of WT) $>$ CB (28%) $>$ BS (25%) $>$ OB (14%)]. Furthermore, we showed that a higher residual CI activity and a less perturbed NADH/NAD⁺ balance correlate with milder metabolic perturbations in *Ndufs4* KO brain regions. Thus, there seems to be a critical threshold (related to the level of redox imbalance and its effect on metabolism) that, when breached, likely limits brain regional capacity to bypass CI deficiency and maintain homeostasis. Glycolysis/gluconeogenesis was markedly enriched in the *Ndufs4* KO olfactory bulbs (FDR- $p < 0.05$), with moderate enrichment ($p < 0.05$) also evident in the other two

lesion-prone brain regions. The *Ndufs4* KO olfactory bulbs additionally displayed marked enrichment of pantothenate and CoA biosynthesis, which was also reflected in the urine metabolome. Moreover, glycine, serine and threonine metabolism were prominently enriched in the cerebellum, urine, and white quadriceps, while glutathione metabolism was more enriched in the anterior cortex and brainstem of *Ndufs4* KO mice. Additionally, *Ndufs4* KO urine also displayed markedly enriched beta-alanine-, glutamine and glutamate-, glyoxylate and dicarboxylate-, tricarboxylic acid (TCA) cycle-, histidine- and butanoate metabolism. In the next sections, we take a deeper look into some of the most prominent similarities and differences among the various *Ndufs4* KO metabolomes.

3.2 Metabolites strongly altered in all *Ndufs4* KO metabolomes

3.2.1 4-Hydroxyproline

Significant reductions in the levels of proline's post-translational product, 4-hydroxyproline, were evident in all *Ndufs4* KO sample types investigated (Fig. 1-B). Since urinary 4-hydroxyproline commonly serves as a bone-resorption biomarker of collagen turnover, decreased renal excretion thereof suggests decreased degradation of collagen from the bone matrix in *Ndufs4* KO mice. In accord, CI deficiency was shown to cause an intrinsic defect in osteoclastogenesis, leading to decreased bone resorption and increased bone mass (osteopetrosis) in *Ndufs4* KO mice (Jin et al., 2014). However, the significant reductions in brain and muscle 4-hydroxyproline levels we report here imply that other sources may also contribute to reduced 4-hydroxyproline excretion. As 4-hydroxyproline is a known pyruvate, glucose, and glycine precursor (Wu et al., 2011), these reductions may reflect its increased utilization in *Ndufs4* KO tissues. Thus, while urinary 4-hydroxyproline may serve as a biomarker for osteopetrosis associated with CI deficiency, its metabolism is also strongly affected in *Ndufs4* KO tissues and warrants further investigation.

3.2.2 2-Amino adipate and lysine catabolism

The precursor for 2-ketoadipate in the lysine catabolic pathway, 2-amino adipate, is another metabolite markedly reduced in all *Ndufs4* KO sample types (Fig. 1-C). The renal excretion of other 2-ketoadipate precursors (5-hydroxylysine, lysine, and tryptophan) and alternative products (2-hydroxyadipate and glutarate) were also significantly reduced in *Ndufs4* KO mice. Additionally, the lysine catabolite, pipecolate, markedly accumulated in brain regions (and muscles) although not measured in urine. As lysine catabolism is dependent on nicotinamide adenine dinucleotide

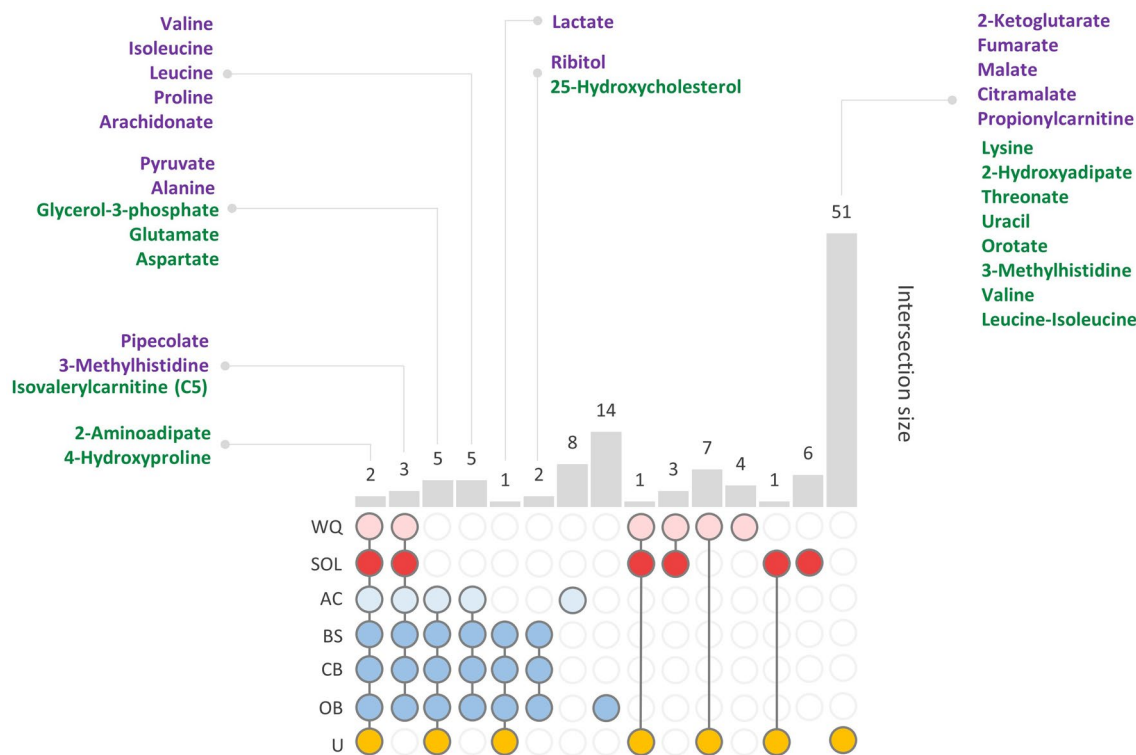


Fig. 2 Intersections of importantly altered metabolites among *Ndufs4* KO sample types. Rows indicate different sample types, while columns correspond to one segment in a Venn diagram. Color filled cells (in columns) indicate the associated samples in a set with empty cells not part of that intersection. Bars indicate the number of unique metabolic alterations per set intersection. Purple and green text respec-

tively indicate significantly ($p<0.05$) increased or decreased metabolite levels in *Ndufs4* KO ($n\geq 19$) mice compared to WTs ($n\geq 20$). Only a few of the relevant metabolic alterations unique to urine are displayed. Abbreviations: AC Anterior cortex, BS Brainstem, CB Cerebellum, OB Olfactory bulbs, SOL Solei, U Urine, WQ White quadriceps

(NAD^+) bioavailability, redox imbalance is one of the main, and well documented, factors linked to MD-related perturbations in this pathway (Esterhuizen et al., 2017). Lysine levels were, however, not as consistently altered with its accumulation only evident in the *Ndufs4* KO olfactory bulbs (and muscles). The degree of lysine accumulation in the olfactory bulbs, further correlated with the accumulation of its metabolite, carnitine, which was also elevated in other brain regions and urine. These observations may point to increased proteolysis in *Ndufs4* KO tissues, as the release of trimethyllysine from cognate proteins is required for endogenous carnitine synthesis, which takes place mainly in the liver, kidneys, and brain but not muscles (Vaz and Wanders, 2002). In support, some of the most significant alterations in *Ndufs4* KO urine were centered around ascorbate (Fig. 1-J), a cofactor required for two dioxygenase reactions in the carnitine biosynthesis pathway. Although urinary ascorbate levels only trended lower, markedly decreased renal excretion of glucarate and gluconate (metabolites from the glucuronate pathway that diverge into the murine ascorbate synthesis pathway) as well as threonate and oxalate (breakdown products of ascorbate) may reflect increased ascorbate demand

in *Ndufs4* KO mice. The enzymes that catalyze these dioxygenase reactions, ϵ -N-trimethyllysine dioxygenase (TMLD, EC 1.14.11.8) and γ -butyrobetaine dioxygenase (BBD, EC 1.14.11.1), also convert 2-ketoglutarate to succinate and perhaps present a favorable alternative route to fuel the ubiquinone (Q)-pool via CII. Furthermore, alterations in ascorbate metabolism may be more evident in the urine metabolome since the expression of BBD is high in the kidneys, moderate in the liver, but low in the brain (Vaz and Wanders, 2002). Marked elevation in brain and muscle levels of 3-methylhistidine (3-MH) and the 3-MH/histidine ratio further support the notion of elevated proteolysis in *Ndufs4* KO tissues (Fig. 1-D). However, the renal excretion of histidine and its methylated derivatives were markedly reduced. These discrepancies confirm previous concerns regarding the use of urinary 3-MH as an index of myofibrillar protein turnover (Shargill et al., 1984; van Goudoever and Matthews, 2017) as several hundred widespread histidine-methylated proteins were recently identified (Davydova et al., 2021; Ning et al., 2016; Wilkinson et al., 2019) and considerable amounts of urinary 3-MH was shown to originate from non-muscle sources (Millward and Bates, 1983; Nishizawa et al., 1977;

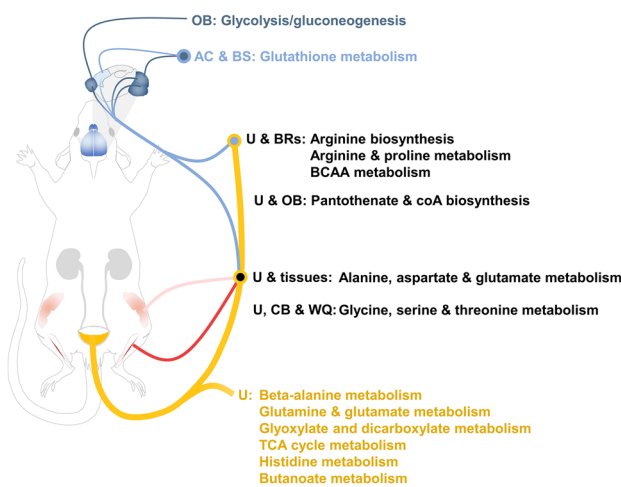


Fig. 3 Affected metabolic pathways in *Ndufs4* KO mice. Significantly enriched pathways identified via pathway over-representation (FDR-adjusted $p<0.05$) analysis. Colored lines represent sample types; while dots indicate intersection of lines and signify commonly affected pathways among sample types. Colors and abbreviations: *AC* Anterior cortex (light blue), *BRs* All brain regions (medium blue), *BS* Brainstem (dark blue), *CB* Cerebellum (dark blue), *OB* Olfactory bulbs (dark blue), *SOL* Solei (red), *U* Urine (yellow), *WQ* White quadriceps (light peach)

Wassner and Li, 1982). Nevertheless, the results reported here not only reveal widespread perturbations in the metabolism of lysine and tryptophan, but also suggest elevated proteolysis and carnitine biosynthesis in a subset of *Ndufs4* KO tissues. Hence, the future investigation of tissue-specific protease activity in *Ndufs4* KO mice is recommended.

3.3 Biofluid markers commonly associated with MD

In *Ndufs4* KO urine, significant elevations were seen in biofluid markers commonly associated with MD i.e., pyruvate, alanine, lactate and the lactate/pyruvate ratio (FDR- $p<0.05$, ES $d=1.20$)—which reflects cytosolic redox state (Esterhuizen et al., 2017; Go et al., 2020; Munnich et al., 1996). These alterations were similar in the brain, which also displayed elevated glycolytic- and pentose phosphate pathway intermediates, with clear differences seen in the degree of metabolite accumulation among regions (Fig. 1–J). The *Ndufs4* KO olfactory bulbs were most significantly affected, while lactate accumulation was only evident in the neurodegeneration-prone brain regions. In agreement, Johnson and colleagues report that pre-symptomatic *Ndufs4* KO mice display significantly elevated levels of pyruvate and lactate along with higher trends in alanine levels in whole brain Johnson et al. (2013) and trended higher levels of glycolytic intermediates and lactate in brain regions, with significant lactate elevation only seen in the olfactory bulbs (Johnson et al., 2020). Contrastingly, reports of blood

lactate levels in *Ndufs4* KO mice vary, with normal, slight, and significant elevation observed (Jain et al., 2016; Jin et al., 2014; Kruse et al., 2008). Considering recent reports of lactate (and not glucose) being the primary circulating TCA substrate for most tissues (except the brain) with the kidneys playing a key role in systemic redox homeostasis by oxidizing lactate to pyruvate (Jang et al., 2019), we suggest that excretory (urine) rather than circulating biofluids may be more appropriate for MD-marker monitoring as the lack of homeostatic control mechanisms in urine allows magnification of metabolic alteration occurring in blood (Wu and Gao, 2015). Similarly, although blood glucose levels are reportedly unaltered in *Ndufs4* KO mice (Kruse et al., 2008), we observed decreased renal excretion of glucose, ribitol, several monosaccharides and sugar acids, suggesting increased glucose utilization in *Ndufs4* KO tissues. In agreement, pyruvate, lactate, and alanine levels all trended lower in *Ndufs4* KO skeletal muscles, possibly indicating increased release thereof to fuel gluconeogenesis. Taken with the accumulation of glycolytic- and pentose phosphate pathway intermediates that we, and others, observed in the *Ndufs4* KO brain as well as reports of upregulated glucose transporter 1 (GLUT1, SLC2A1) protein levels in the *Ndufs4* KO brain (Lee et al., 2019) and pro-glycolysis genes in the *Ndufs4* KO liver (Jin et al., 2014), we postulate that glucose production, uptake and utilization is elevated in *Ndufs4* KO mice.

In agreement with our observations, muscle lactate levels in patients with mitochondrial disease, was shown to be lower at rest but elevated during exercise (Lindholm et al., 2004; Löfberg et al., 2001). Another possible explanation for this discrepancy between *Ndufs4* KO muscle and brain metabolomes is the activity of the glycerol-3-phosphate (G3P) shuttle, which is one of the most important, highly active redox regulatory shuttles in skeletal muscle that has limited activity in the brain (Liu et al., 2021; Schiaffino and Reggiani, 2011). Increased G3P synthesis (and shuttle activity) is known to reduce muscle lactate build-up (Alfadda et al., 2004) and was recently shown to be an important endogenous NAD⁺-regeneration pathway during CI inhibition that suppresses neuroinflammation and extends lifespan when enhanced in *Ndufs4* KO mice (Liu et al., 2021). Interestingly, mice with cytosolic G3P dehydrogenase (cGPD; EC 1.1.1.8) deficiency display increased dihydroxy acetone phosphate (DHAP) and decreased G3P in muscle (MacDonald and Marshall, 2000, 2001), similar to what we observed in *Ndufs4* KO brain regions—suggesting that there may be an increased need for this shuttle in brain during CI deficiency. In agreement, lower levels of G3P and an increased trend in DHAP levels could also be seen in the whole-brain metabolomics data from pre-symptomatic *Ndufs4* KO mice (Johnson et al., 2013). Although we could not detect these metabolites in muscles, urinary G3P excretion was markedly

decreased in *Ndufs4* KO mice. In addition, TCA cycle-linked metabolites (succinate and 2-hydroxyglutarate) which, like G3P, can fuel the Q-pool independently of CI, were consistently and significantly decreased in *Ndufs4* KO brain regions and urine. The accumulation of TCA cycle intermediates, 2-ketoglutarate, fumarate, and malate in biofluids is another metabolic signature characteristic of MD, that suggests TCA cycle congestion. Although these metabolites were significantly elevated in *Ndufs4* KO urine, they were not markedly altered in the various brain regions (Fig. 1-F). Others have also reported early-stage elevations in fumarate levels in affected brain regions (but not muscle) of *Ndufs4* KO mice, which was not evident in brain regions of older mice (Piroli et al., 2020; Piroli et al., 2016). Overall, urine proves to be a fitting biofluid with which to monitor classic MD biomarkers that reflect the redox state in affected brain regions. However, with inconsistencies between tissue and urine levels of TCA cycle intermediates observed, questions arise regarding the extent of TCA cycle congestion in individual *Ndufs4* KO tissues.

3.4 Inconsistent alterations between systemic and brain region-specific metabolomes

3.4.1 BCAA catabolism

BCAAs, valine, leucine, and isoleucine markedly accumulated in *Ndufs4* KO lesion-prone brain regions, with elevations also evident in the lesion-resistant anterior cortex (Fig. 1-G). The degree of these elevations correlated with reductions in leucine's catabolic by-product, isovalerylcarnitine (C5). Although these alterations were not observed in whole brain or brain regions of pre-symptomatic mice (Johnson et al., 2020; Johnson et al., 2013), perturbations in BCAA catabolism have been reported in MD cases and, as with lysine, is believed to result from the redox imbalance associated with MD (Esterhuizen et al., 2017). Several tissues jointly control BCAA catabolism, with skeletal muscle and liver playing a central role (Holeček, 2018). The first step in BCAA catabolism primarily occurs in skeletal muscles, which then release most branched-chain keto acids (along with glutamine and alanine) into circulation to be taken up by other tissues (Harper et al., 1984). BCAA levels were not significantly altered in skeletal muscles, but trended lower in the glycolytic white quadriceps, while the renal excretion of BCAAs (and their metabolites) were markedly decreased in *Ndufs4* KO mice. Taken together, these observations suggest that an increased influx of BCAA in the brain, together with a restriction in the NAD⁺-dependent step of BCAA catabolism, may result in elevated BCAA levels. Furthermore, we postulate that BCAA catabolism could be enhanced in a subset of *Ndufs4* KO tissues, possibly to fuel succinyl-CoA production and the Q-pool via

electron-transferring-flavoprotein dehydrogenase (ETFDH, EC 1.5.5.1). Such a tissue-specific difference in BCAA handling has also been proposed to take place in insulin resistant individuals (Newgard, 2012).

3.4.2 Aspartate, glutamate, and arginine metabolism

Glutamate (Glu), pyroglutamate, and aspartate levels were significantly decreased in *Ndufs4* KO brain regions and urine (Fig. 1-A). Among these, the degree of aspartate reduction was greater in the brain, in which asparagine levels were also markedly lower. In accord, pre-symptomatic *Ndufs4* KO mice display trended lower brain-regional levels of a metabolite cluster including Glu, pyroglutamate, aspartate, and ornithine as well as decreased trends in whole brain levels of 3-aminobutyrate and most free amino acids, (Johnson et al., 2020). We additionally observed significant reductions in glutamine (Gln) and 3-aminobutyrate abundance in *Ndufs4* KO urine but not brain regions. Furthermore, alterations in aspartate and Glu metabolism were consistent in *Ndufs4* KO urine and white quadriceps, although less significant in the muscles. These observations could reflect a systemic increase in Gln and Glu consumption, a phenomenon which has recently been linked to compensatory mechanisms that function to decrease mitochondrial redox stress during OXPHOS deficiency. Enhanced Gln-derived anaplerosis of the TCA cycle was shown to regenerate NAD⁺ via aspartate efflux from mitochondria, however, when the level of OXPHOS deficiency exceeds a certain threshold, Gln starts fueling acetylation and lipogenesis via reductive carboxylation (Chen et al., 2018). Similarly, enhanced Gln-derived proline biosynthesis was shown to regenerate NAD(P)⁺ levels when TCA cycle activity surpasses OXPHOS capacity (Schwörer et al., 2020). While the former mechanism may be a systemic adaption, the latter seems to be exclusive to the *Ndufs4* KO brain, where proline levels were uniquely elevated (Fig. 1B). The marked decrease in urine and muscle proline levels further confirm that this putative phenomenon is not systemic. On the contrary, Yang et al. (2020) recently reported a marked decrease in circulatory Gln turnover flux and Gln anaplerosis in the pancreas and liver of *Ndufs4* KO mice, while Gln's contribution to (or handling within) the TCA cycle did not markedly alter in other tissues. Our results further indicate a significant decrease in the renal excretion of N-acetylglutamate (NAG) and other urea cycle intermediates (carbamate, ornithine, citrulline, arginine, and urate) in *Ndufs4* KO mice, with the urinary alanine/Glu- and Glu/Gln ratios elevated (FDR-*p*<0.05, ES *d*>1.2). Although citrulline levels consistently trended lower in *Ndufs4* KO brain regions (and muscles), the degree and direction of other alterations in arginine metabolism were inconsistent. Contrastingly, most of these metabolites were moderately elevated in both glycolytic and oxidative muscles. Taken

together with the alterations described in previous sections, this might reflect increased muscle proteolysis and amino acid catabolism along with increased ammonia transfer to the liver. Elevated levels of NAG (brain regions) and N-acetylglutamate (muscles) further suggest increased protein acetylation in *Ndufs4* KO tissues.

3.4.3 Lipid metabolism

The levels of glycerol along with several carnitine- and glycine conjugated medium chain fatty acids (hexanoyl-, octanoyl- and decanoylcarnitine; butyryl-, valeryl- and hexanoylglycine) were decreased in *Ndufs4* KO urine (and muscle). Glycerol levels were variably affected among *Ndufs4* KO brain regions, while the levels of fatty acids, palmitate (C16:0), oleate (C18:1), and arachidonate (C20:4, ω-6) consistently trended higher (Fig. 1-E). Cytosolic acetyl-CoA accumulation is known to stimulate lipogenesis, cholesterol synthesis and protein acetylation (Pietrocola et al., 2015; Saggesson, 2008). Significant elevations were seen in the renal excretion and tissue content of acetylcarnitine, which suggest acetyl-CoA accumulation in *Ndufs4* KO mice, as this membrane permeant storage form of acetyl-CoA serves to dispose of or replenish it as needed (Schroeder et al., 2012). Additionally, the olfactory bulbs, which was most markedly affected, displayed decreased levels of pantothenate (a CoA component) and its precursor, beta-alanine—likely reflecting increased CoA demand. In lesion-prone brain regions, significant reductions were also evident in the levels of 25-hydroxycholesterol, which like arachidonate, has been described to play a regulatory role in cholesterol metabolism (Demetz et al., 2014; Kilsdonk et al., 1995). Interestingly, increasing cholesterol production, export, and utilization was recently shown to attenuate elevated NAD(P)H levels in CI deficient fibroblast (Schirris et al., 2021). Recent reports of protein hyper-acetylation (Gella et al., 2020; Piroli et al., 2020) and increased lipid synthesis in lesion-prone brain regions (Liu et al., 2017; Liu et al., 2015) as well as elevated levels of triacylglycerol and free fatty acids in the serum of *Ndufs4* KO mice (Jin et al., 2014) further support the notion of acetyl-CoA accumulation and increased lipogenesis in *Ndufs4* KO brain regions (Chen et al., 2018; Mullen et al., 2014; Yang et al., 2014). Taken together with the observations discussed in previous sections, the data points to a systemic mismatch between the amount of acetyl-CoA generated via catabolic reactions in *Ndufs4* KO tissues and the processing capacity of the TCA cycle.

3.4.4 Choline-, one-carbon-, and nucleotide metabolism

Decreased levels of intermediates in the metabolism of choline to glycine i.e., trimethylglycine (betaine), dimethylglycine and methylglycine (sarcosine) along with methionine,

and cystathione were among the most significant alterations observed in *Ndufs4* KO urine (Fig. 1-H). Although not as evident in the brain, these alterations were mirrored in the *Ndufs4* KO white quadriceps. Choline-derived betaine remethylates homocysteine to methionine in the methionine cycle, with the subsequent oxidation of dimethylglycine and sarcosine both feeding the Q-pool via ETFDH and ultimately producing glycine. Betaine mainly serves as a methyl donor in the liver, where betaine-homocysteine methyltransferase (BHMT, EC 2.1.1.5) is highly expressed (Szegedi et al., 2008; Teng et al., 2011). In addition to the liver, renal metabolism is also thought to play an important role in systemic one-carbon (1C) homeostasis, as the kidneys produce the bulk of systemic serine and glycine (Jang et al., 2019). Decreased renal excretion of glycine, serine, histidine, threonine, and cystine in *Ndufs4* KO mice further suggests significant perturbations in hepatic and renal 1C metabolism. Despite discrepancies among *Ndufs4* KO brain regions, betaine and serine levels consistently trend lower (except in the olfactory bulbs) with glycine markedly elevated in the brainstem and reduced in the cerebellum.

Marked reductions in some purine and pyrimidine intermediates were also evident in the olfactory bulbs and anterior cortex (Fig. 1-I). In agreement, significantly decreased renal excretion of purine- and pyrimidine catabolism end-products, urate and beta-alanine, were observed in *Ndufs4* KO mice along with decreased levels of orotate, uracil, 3-ureidopropionate, and thymine cabolite, 3-amino-isobutyrate. In accordance, nucleotides and products of nucleotide catabolism were also decreased in whole brain of pre-symptomatic *Ndufs4* KO mice (Johnson et al., 2013). As purine and pyrimidine nucleotides are important precursors for the synthesis of nucleotide cofactors such as NAD⁺ and S-adenosyl methionine (SAM), these alterations are likely linked to perturbations in redox balance and 1C metabolism. Several studies have functionally linked 1C metabolism and serine catabolism, specifically, to the OXPHOS system and deficiencies thereof (Bao et al., 2016; Lucas et al., 2018; Nikkanen et al., 2016); with a maladaptive increase in the fraction of NADH produced by folate-mediated serine catabolism recently reported in *Ndufs4* KO mice (Yang et al., 2020). Altogether, our data shows that serine-, 1C-, and nucleotide- metabolism is markedly perturbed in *Ndufs4* KO mice, with the methylation cycle most dramatically affected. While these alterations in the urine metabolome likely reflect hepatic and renal metabolism, 1C-metabolism linked perturbations are also evident in *Ndufs4* KO brain regions and muscles.

3.5 Contributions of gut microbial metabolism

Several metabolic alterations in *Ndufs4* KO urine seemed to reflect altered gut microbial metabolism (Fig. S2). This

includes significantly elevated levels of 2,3-butandiol, 2,6-dihydroxybenzoate, citramalate, and propionylcarnitine along with decreased levels of 3-hydroxyphenyl (HP) propanoate, 4-HP-glycolate, 4-HP-acetate, and 4-HP-pyruvate. 2,3-Butandiol is known to accumulate in the urine of MD patients and thought to reflect high systemic levels of glucose that is further metabolized by gut microbes (Elshaghabee et al., 2016; Esterhuizen et al., 2019; Venkataraman et al., 2014). Gut microbiota are also major producers of short chain fatty acids (SCFs), especially propionate and butyrate (Jang et al., 2019). Therefore, markedly altered SCF acyl-conjugates in *Ndufs4* KO mice may be related to intestinal metabolism. It was recently shown that gut microbiota can metabolize host-derived lactate to SCFs, predominantly propionate, which can then cross back into the host (Scheiman et al., 2019). Since propionylcarnitine levels were decreased in most *Ndufs4* KO brain regions (and muscles), the urinary accumulation of propionylcarnitine is likely related to lactate accumulation in *Ndufs4* KO mice and gut-derived elevations in propionate. In support, increased urinary citramalate excretion is also seen with propionyl-CoA accumulation (in propionyl-CoA carboxylase deficiency) and is associated with intestinal dysbiosis (Greter et al., 1980). Furthermore, reduced urinary excretion of 4-HP-acetate and 4-HP-pyruvate may reflect perturbations in host-microbial co-metabolism of aromatic amino acids (Li et al., 2021). This is supported by decreased levels of phenylalanine, tryptophan, kynurene, and 5-hydroxy-indole exclusively in *Ndufs4* KO urine. Alterations in gut microbiota have been reported in a variety of disease phenotypes with this host-gut microbiota interaction recently linked to changes in mitochondrial function and redox status (Yardeni et al., 2019). Accordingly, our data indicates that altered microbial compositions or metabolism likely contribute to metabolic observations in biofluids of LS patients. Furthermore, it must be noted that when working with mouse models, microbiota transfer between mice via coprophagy could influence metabolomes when genotypes are cohoused—as was done in this study. Although the ingestion of feces by self-grooming is considered more probable, the transfer of microbiota between genotypes cannot be ruled out and measures should be taken to avoid this (Brinkman et al., 2013; Laukens et al., 2016). Together, these observations highlight the necessity of future studies investigating host-bacterial co-metabolism and the gut-brain axis in LS.

4 Conclusions

Here, we integrate and cross-compare multi-platform metabolomics data from urine and tissues of late stage diseased *Ndufs4* KO vs WT mice to better understand how systemic biofluids reflect tissue-specific metabolic alterations in

LS. We confirm that biofluid markers associated with MD (elevated alanine, pyruvate, and lactate) and several other metabolic signatures in urine reflect metabolic alterations in the LS brain, thereby verifying the value of urine for the monitoring of these metabolic markers. In addition to glycolytic and TCA cycle intermediates, it would be advantageous to investigate (and validate) whether the following urinary metabolites could serve as biomarkers of LS and MD: amino acids and derivatives related to alanine, aspartate and glutamate-; arginine and proline-; BCAA-; lysine-; histidine-; and choline metabolism; as well as sugar derivatives; metabolites related to the G3P shuttle; and gut microbial metabolism. Widespread reductions were evident in the abundance of several metabolites capable of fueling Q-pool linked dehydrogenases (other than CI) in *Ndufs4* KO mice, therefore, we hypothesize that tissue-specific differences in these dehydrogenases could influence metabolic flexibility and the consequences of CI deficiency in different tissues. Our data further reveals that impaired BCAA catabolism, increased proline biosynthesis, and the accumulation of glycolytic intermediates are brain-specific metabolic perturbations in LS. Contrastingly, elevated levels of TCA cycle intermediates in urine, and significant reductions in one-carbon metabolism intermediates, are not clearly reflected in the *Ndufs4* KO brain and appear to be systemic of origin. Furthermore, the discrepancies we report between urinary and tissue-specific metabolomes highlight the shortcomings of only using systemic biofluids as an investigative tool for multi-systemic diseases. Although non- or minimally invasive systemic samples contain valuable information, these metabolomes should be carefully interpreted in conjunction with tissue-specific data—especially when aiming to elucidate disease mechanisms. In this regard, having reliable MD models and access tissue samples that cannot be obtained from patients, is vital to improve our understanding of complex MD processes. Additionally, future sex-specific studies, targeting the areas of metabolism identified here, should be a priority. Almost all aspects of metabolism and energy homeostasis are regulated in a sex-specific manner, which influences disease pathogenesis. Sex hormones and -chromosomes along with differences in tissue-specific gene regulation and gut microbiota between sexes play a central role in this metabolic sexual dimorphism (Chella Krishnan et al., 2018; Clegg and Mauvais-Jarvis, 2018). Indeed, many metabolic pathways affected in male *Ndufs4* KO mice, have been shown to display sexual dimorphism in murine models and/or humans. This includes glucose and lipid metabolism (Baars et al., 2018; Chella Krishnan et al., 2018; Clegg and Mauvais-Jarvis, 2018; Lundsgaard and Kiens, 2014), amino acid and acylcarnitine metabolism (Ruoppolo et al., 2018; Wu and Gao, 2015), branched-chain amino acid metabolism (Vignoli et al., 2018), and bone metabolism (Choi et al., 2021).

Supplementary Information The online version contains supplementary material available at <https://doi.org/10.1007/s11306-021-01854-8>.

Acknowledgements We thank W. Horak and J. Coetzer for their assistance with the metabolomics analyses as well as K. Venter and A. Fick, from the Pre-Clinical Drug Development Platform (PCDDP, NWU, RSA), for their assistance regarding animal handling.

Author contributions KT and RL designed the research plan with input from JZL and FvdW. FvdW acquired the animal model and ethical approval with assistance from RL. RL and FvdW obtained funding for the study. KT performed the data processing with assistance from RL and JZL. KT analyzed the data and wrote the manuscript with input from RL, JZL and FvdW.

Funding This work was supported by the National Research Foundation of South Africa (NRF, Grant No. 92736, 108146, 111479 and 121368), the Technology Innovation Agency of the Department of Science and Technology of South Africa (TIA, Grant No. Metabol. 01), and the North-West University (NWU). Opinions expressed and conclusions arrived at, are those of the authors and are not necessarily to be attributed to the NRF, TIA or NWU.

Data availability The metabolomics data obtained in this study can be accessed at the Common Fund's National Metabolomics Data Repository (NMDR) website, the Metabolomics Workbench (<https://www.metabolomicsworkbench.org>) where it has been assigned project IDs: PR000721 (Terburgh et al., 2019a), PR001003 (Terburgh et al., 2021b), and PR001187 (Terburgh et al., 2021c).

Declarations

Conflict of interest The authors declare no conflict of interest.

Ethical approval The AnimCare animal research ethics committee of North-West University approved (NWU-0001-15-A5 and NWU-00378-16-A5) the animal protocols used in this study. All animals were maintained, and all procedures performed, in accordance with the code of ethics in research, training, and testing of drugs in South Africa and complied with national legislation.

References

- Alam, M. T., Manjeri, G. R., Rodenburg, R. J., Smeitink, J. A. M., Notebaart, R. A., Huynen, M., Willems, P. H. G. M., & Koopman, W. J. H. (2015). Skeletal muscle mitochondria of NDUFS4^{-/-} mice display normal maximal pyruvate oxidation and ATP production. *Biochim. Biophys. Acta Bioenerg.*, 1847, 526–533.
- Alfadda, A., DosSantos, R. A., Stepanyan, Z., Marrif, H., & Silva, J. E. (2004). Mice with deletion of the mitochondrial glycerol-3-phosphate dehydrogenase gene exhibit a thrifty phenotype: Effect of gender. *Am. J. Physiol. Regul. Integr. Comp. Physiol.*, 287, R147–R156.
- Baars, A., Oosting, A., Lohuis, M., Koehorst, M., El Aidy, S., Hugenholtz, F., Smidt, H., Mischke, M., Boekschooten, M. V., Verkade, H. J., Garssen, J., van der Beek, E. M., Knol, J., de Vos, P., van Bergenhenegouwen, J., & Fransen, F. (2018). Sex differences in lipid metabolism are affected by presence of the gut microbiota. *Sci. Rep.*, 8, 13426.
- Bao, X. R., Ong, S.-E., Goldberger, O., Peng, J., Sharma, R., Thompson, D. A., Vafai, S. B., Cox, A. G., Marutani, E., Ichinose, F., Goessling, W., Regev, A., Carr, S. A., Clish, C. B., & Mootha, V. K. (2016). Mitochondrial dysfunction remodels one-carbon metabolism in human cells. *eLife*, 5, e10575.
- Bolea, I., Gella, A., Sanz, E., Prada-Dacasa, P., Menard, F., Bard, A. M., Rquez, P.M.-M., Eraso-Pichot, A., dol-Caballero, G. M., Navarro, X., Kalume, F., & Quintana, A. (2019). Defined neuronal populations drive fatal phenotype in a mouse model of Leigh syndrome. *eLife*, 8, e47163.
- Brinkman, B. M., Becker, A., Ayiseh, R. B., Hildebrand, F., Raes, J., Huys, G., & Vandenebeele, P. (2013). Gut microbiota affects sensitivity to acute DSS-induced colitis independently of host genotype. *Inflamm. Bowel. Dis.*, 19, 2560–7.
- Chella Krishnan, K., Mehrabian, M., & Lusis, A. J. (2018). Sex differences in metabolism and cardiometabolic disorders. *Curr. Opin. Lipidol.*, 29, 404–410.
- Chen, Q., Kirk, K., Shurubor, Y. I., Zhao, D., Arreguin, A. J., Shahi, I., Valsecchi, F., Primiano, G., Calder, E. L., & Carelli, V. (2018). Rewiring of glutamine metabolism is a bioenergetic adaptation of human cells with mitochondrial DNA mutations. *Cell Metab.*, 27, 1007–1025.e5.
- Choi, K. H., Lee, J. H., & Lee, D. G. (2021). Sex-related differences in bone metabolism in osteoporosis observational study. *Medicine*, 100, e26153.
- Chong, J., Soufan, O., Li, C., Caraus, I., Li, S., Bourque, G., Wishart, D. S., & Xia, J. (2018). MetaboAnalyst 4.0: Towards more transparent and integrative metabolomics analysis. *Nucleic Acids Res.*, 46, W486–W494.
- Chouchani, E. T., Methner, C., Buonincontri, G., Hu, C.-H., Logan, A., Sawiak, S. J., Murphy, M. P., & Krieg, T. (2014). Complex I deficiency due to selective loss of Ndufs4 in the mouse heart results in severe hypertrophic cardiomyopathy. *PLoS One*, 9, e94157.
- Clegg, D. J., & Mauvais-Jarvis, F. (2018). An integrated view of sex differences in metabolic physiology and disease. *Mol. Metab.*, 15, 1–2.
- Davydova, E., Shimazu, T., Schuhmacher, M. K., Jakobsson, M. E., Willemen, H. L. D. M., Liu, T., Moen, A., Ho, A. Y. Y., Malecki, J., Schroer, L., Pinto, R., Suzuki, T., Grønsberg, I. A., Sohtome, Y., Akakabe, M., Weirich, S., Kikuchi, M., Olsen, J. V., Dohmae, N., ... Falnes, P. Ø. (2021). The methyltransferase METTL9 mediates pervasive 1-methylhistidine modification in mammalian proteomes. *Nat. Commun.*, 12, 891.
- Demetz, E., Schroll, A., Auer, K., Heim, C., Patsch, J. R., Eller, P., Theurl, M., Theurl, I., Theurl, M., Seifert, M., Lener, D., Stanzl, U., Haschka, D., Asshoff, M., Dichtl, S., Nairz, M., Huber, E., Stadlinger, M., Moschen, A. R., ... Tancevski, I. (2014). The arachidonic acid metabolome serves as a conserved regulator of cholesterol metabolism. *Cell Metab.*, 20, 787–798.
- Di Meo, I., Marchet, S., Lamperti, C., Zeviani, M., & Visconti, C. (2017). AAV9-based gene therapy partially ameliorates the clinical phenotype of a mouse model of Leigh syndrome. *Gene Ther.*, 24, 661–667.
- Elshaghabee, F. M., Bockelmann, W., Meske, D., de Vreese, M., Walte, H. G., Schrezenmeir, J., & Heller, K. J. (2016). Ethanol production by selected intestinal microorganisms and lactic acid bacteria growing under different nutritional conditions. *Front. Microbiol.*, 7, 47.
- Emmerzaal, T. L., Preston, G., Geenen, B., Verweij, V., Wiesmann, M., Vasileiou, E., Grüter, F., de Groot, C., Schoorl, J., de Veer, R., Roelofs, M., Arts, M., Hendriksen, Y., Klimars, E., Donti, T. R., Graham, B. H., Morava, E., Rodenburg, R. J., & Kozicz, T. (2020). Impaired mitochondrial complex I function as a candidate driver in the biological stress response and a concomitant stress-induced brain metabolic reprogramming in male mice. *Transl. Psychiatry*, 10, 176.
- Esterhuizen, K., Lindeque, J. Z., Mason, S., van der Westhuizen, F. H., Suomalainen, A., Hakonen, A. H., Carroll, C. J., Rodenburg,

- R. J., de Laat, P. B., Janssen, M. C. H., Smeitink, J. A. M., & Louw, R. (2019). A urinary biosignature for mitochondrial myopathy, encephalopathy, lactic acidosis and stroke like episodes (MELAS). *Mitochondrion*, 45, 38–45.
- Esterhuizen, K., van der Westhuizen, F. H., & Louw, R. (2017). Metabolomics of mitochondrial disease. *Mitochondrion*, 35, 97–110.
- Gella, A., Prada-Dacasa, P., Carrascal, M., Urpi, A., González Torres, M., Abian, J., Sanz, E., & Quintana, A. (2020). Mitochondrial proteome of affected glutamatergic neurons in a mouse model of Leigh syndrome. *Front. Cell Dev. Biol.*, 8, 660.
- Go, S., Kramer, T. T., Verhoeven, A. J., Oude Elferink, R. P. J., & Chang, J.-C. (2020). The extracellular lactate-to-pyruvate ratio modulates the sensitivity to oxidative stress-induced apoptosis via the cytosolic NADH/NAD⁺ redox state. *Apoptosis*, 26, 38–51.
- Greter, J., Lindstedt, S., Seeman, H., & Steen, G. (1980). 2-Hydroxy-2-methylsuccinic acid—a urinary metabolite in propionyl-CoA carboxylase deficiency. *Clin. Chim. Acta*, 106, 103–106.
- Gullberg, J., Jonsson, P., Nordström, A., Sjöström, M., & Moritz, T. (2004). Design of experiments: An efficient strategy to identify factors influencing extraction and derivatization of *Arabidopsis thaliana* samples in metabolomic studies with gas chromatography/mass spectrometry. *Anal. Biochem.*, 331, 283–295.
- Harper, A. E., Miller, R. H., & Block, K. P. (1984). Branched-chain amino acid metabolism. *Annu. Rev. Nutr.*, 4, 409–54.
- Holeček, M. (2018). Branched-chain amino acids in health and disease: Metabolism, alterations in blood plasma, and as supplements. *Nutr. Metab.*, 15, 33–33.
- Ito, T. K., Lu, C., Khan, J., Nguyen, Q., Huang, H. Z., Kim, D., Phillips, J., Tan, J., Lee, Y., Nguyen, T., Khessib, S., Lim, N., Mekvanich, S., Oh, J., Pineda, V. V., Wang, W., Bitto, A., An, J. Y., Morton, J. F., ... Kaeberlein, M. (2017). Hepatic S6K1 partially regulates lifespan of mice with mitochondrial complex I deficiency. *Front. Genet.*, 8, 113.
- Jain, I. H., Zazzeron, L., Goli, R., Alexa, K., Schatzman-Bone, S., Dhillon, H., Goldberger, O., Peng, J., Shalem, O., Sanjana, N. E., Zhang, F., Goessling, W., Zapol, W. M., & Mootha, V. K. (2016). Hypoxia as a therapy for mitochondrial disease. *Science*, 352, 54–61.
- Jang, C., Hui, S., Zeng, X., Cowan, A. J., Wang, L., Chen, L., Morscher, R. J., Reyes, J., Frezza, C., Hwang, H. Y., Imai, A., Saito, Y., Okamoto, K., Vaspoli, C., Kasprinski, L., Zsido, G. A., Gorman, J. H., Gorman, R. C., & Rabinowitz, J. D. (2019). Metabolite exchange between mammalian organs quantified in pigs. *Cell Metab.*, 30, 594–606.e3.
- Jin, Z., Wei, W., Yang, M., Du, Y., & Wan, Y. (2014). Mitochondrial complex I activity suppresses inflammation and enhances bone resorption by shifting macrophage-osteoclast polarization. *Cell Metab.*, 20, 483–498.
- Johnson, S. C., Kayser, E.-B., Bornstein, R., Stokes, J., Bitto, A., Park, K. Y., Pan, A., Sun, G., Raftery, D., Kaeberlein, M., Sedensky, M. M., & Morgan, P. G. (2020). Regional metabolic signatures in the Ndufs4(KO) mouse brain implicate defective glutamate/α-ketoglutarate metabolism in mitochondrial disease. *Mol. Genet. Metab.*, 130, 118–132.
- Johnson, S. C., Yanos, M. E., Kayser, E. B., Quintana, A., Sangesland, M., Castanza, A., Uhde, L., Hui, J., Wall, V. Z., Gagnidze, A., Oh, K., Wasko, B. M., Ramos, F. J., Palmiter, R. D., Rabinovitch, P. S., Morgan, P. G., Sedensky, M. M., & Kaeberlein, M. (2013). mTOR inhibition alleviates mitochondrial disease in a mouse model of Leigh syndrome. *Science*, 342, 1524–1528.
- Kilsdonk, E. P., Morel, D. W., Johnson, W. J., & Rothblat, G. H. (1995). Inhibition of cellular cholesterol efflux by 25-hydroxycholesterol. *J. Lipid Res.*, 36, 505–516.
- Kruse, S. E., Watt, W. C., Marcinek, D. J., Kapur, R. P., Schenkman, K. A., & Palmiter, R. D. (2008). Mice with mitochondrial complex I deficiency develop a fatal encephalomyopathy. *Cell Metab.*, 7, 312–320.
- Lake, N. J., Compton, A. G., Rahman, S., & Thorburn, D. R. (2016). Leigh syndrome: One disorder, more than 75 monogenic causes. *Ann. Neurol.*, 79, 190–203.
- Laukens, D., Brinkman, B. M., Raes, J., De Vos, M., & Vandenebeeke, P. (2016). Heterogeneity of the gut microbiome in mice: Guidelines for optimizing experimental design. *FEMS microbiology reviews*, 40, 117–132.
- Lee, C. F., Caudal, A., Abell, L., Nagana Gowda, G. A., & Tian, R. (2019). Targeting NAD(+) metabolism as interventions for mitochondrial disease. *Sci. Rep.*, 9, 3073–3073.
- Li, J. V., Ashrafi, H., Sarafian, M., Homola, D., Rushton, L., Barker, G., Cabrera, P. M., Lewis, M. R., Darzi, A., Lin, E., Gletsu-Miller, N. A., Atkin, S. L., Sathyapalan, T., Gooderham, N. J., Nicholson, J. K., Marchesi, J. R., Athanasiou, T., & Holmes, E. (2021). Roux-en-Y gastric bypass-induced bacterial perturbation contributes to altered host-bacterial co-metabolic phenotype. *Microbiome*, 9, 139.
- Lindholm, H., Löfberg, M., Somer, H., Näveri, H., & Sovijärvi, A. (2004). Abnormal blood lactate accumulation after exercise in patients with multiple mitochondrial DNA deletions and minor muscular symptoms. *Clin. Physiol. Funct. Imaging*, 24, 109–15.
- Liu, L., MacKenzie, K. R., Putluri, N., Maletić-Savatić, M., & Bellen, H. J. (2017). The glia-neuron lactate shuttle and elevated ROS promote lipid synthesis in neurons and lipid droplet accumulation in glia via APOE/D. *Cell Metab.*, 26, 719–737.e6.
- Liu, L., Zhang, K., Sandoval, H., Yamamoto, S., Jaiswal, M., Sanz, E., Li, Z., Hui, J., Graham, B. H., & Quintana, A. (2015). Glial lipid droplets and ROS induced by mitochondrial defects promote neurodegeneration. *Cell*, 160, 177–190.
- Liu, S., Fu, S., Wang, G., Cao, Y., Li, L., Li, X., Yang, J., Li, N., Shan, Y., Cao, Y., Ma, Y., Dong, M., Liu, Q., & Jiang, H. (2021). Glycerol-3-phosphate biosynthesis regenerates cytosolic NAD⁺ to alleviate mitochondrial disease. *Cell Metab.* <https://doi.org/10.1016/j.cmet.2021.06.013>
- Löfberg, M., Lindholm, H., Näveri, H., Majander, A., Suomalainen, A., Paetau, A., Sovijärvi, A., Häkkinen, M., & Somer, H. (2001). ATP, phosphocreatine and lactate in exercising muscle in mitochondrial disease and McArdle's disease. *Neuromuscul. Disord.*, 11, 370–5.
- Lucas, S., Chen, G., Aras, S., & Wang, J. (2018). Serine catabolism is essential to maintain mitochondrial respiration in mammalian cells. *Life Sci. Alliance*, 1, e201800036.
- Lundsgaard, A. -M., & Kiens, B. (2014). Gender differences in skeletal muscle substrate metabolism – molecular mechanisms and insulin sensitivity. *Frontiers in Endocrinology*, 5.
- MacDonald, M. J., & Marshall, L. K. (2000). Mouse lacking NAD+-linked glycerol phosphate dehydrogenase has normal pancreatic beta cell function but abnormal metabolite pattern in skeletal muscle. *Arch. Biochem. Biophys.*, 384, 143–153.
- MacDonald, M. J., & Marshall, L. K. (2001). Survey of normal appearing mouse strain which lacks malic enzyme and Nad+-linked glycerol phosphate dehydrogenase: Normal pancreatic beta cell function, but abnormal metabolite pattern in skeletal muscle. *Mol. Cell. Biochem.*, 220, 117–125.
- Miller, H. C., Louw, R., Mereis, M., Venter, G., Boshoff, J.-D., Mienie, L., van Reenen, M., Venter, M., Lindeque, J. Z., Domínguez-Martínez, A., Quintana, A., & van der Westhuizen, F. H. (2021). Metallothionein 1 overexpression does not protect against mitochondrial disease pathology in Ndufs4 knockout mice. *Mol. Neurobiol.*, 58, 243–262.
- Millward, D. J., & Bates, P. C. (1983). 3-Methylhistidine turnover in the whole body, and the contribution of skeletal muscle and intestine to urinary 3-methylhistidine excretion in the adult rat. *Biochem. J.*, 214, 607–615.

- Mootha, V. K., & Chinnery, P. F. (2018). Oxygen in mitochondrial disease: Can there be too much of a good thing? *J. Inherit. Metab. Dis.*, *41*, 761–763.
- Mullen, Andrew R., Hu, Z., Shi, X., Jiang, L., Boroughs, Lindsey K., Kovacs, Z., Boriack, R., Rakheja, D., Sullivan, Lucas B., Linehan, W. M., Chandel, Navdeep S., & DeBerardinis, Ralph J. (2014). Oxidation of alpha-ketoglutarate is required for reductive carboxylation in cancer cells with mitochondrial defects. *Cell Rep.*, *7*, 1679–1690.
- Munnich, A., Rötig, A., Chretien, D., Saudubray, J. M., Cormier, V., & Rustin, P. (1996). Clinical presentations and laboratory investigations in respiratory chain deficiency. *Eur. J. Pediatr.*, *155*, 262–274.
- Newgard, C. B. (2012). Interplay between lipids and branched-chain amino acids in development of insulin resistance. *Cell Metab.*, *15*, 606–614.
- Nikkanen, J., Forsstrom, S., Euro, L., Paetau, I., Kohnz, R. A., Wang, L., Chilov, D., Viinamaki, J., Roivainen, A., Marjamaki, P., Liljenback, H., Ahola, S., Buzkova, J., Terzioglu, M., Khan, N. A., Pirnes-Karhu, S., Paetau, A., Lonnqvist, T., Sajantila, A., ... Suomalainen, A. (2016). Mitochondrial DNA replication defects disturb cellular dNTP pools and remodel one-carbon metabolism. *Cell Metab.*, *23*, 635–648.
- Ning, Z., Star, A. T., Mierzwa, A., Lanouette, S., Mayne, J., Couture, J.-F., & Figgeys, D. (2016). A charge-suppressing strategy for probing protein methylation. *Chem. Commun.*, *52*, 5474–5477.
- Nishizawa, N., Noguchi, T., Hareyama, S., & Funabiki, R. (1977). Fractional flux rates of N τ -methylhistidine in skin and gastrointestinal: The contribution of these tissues to urinary excretion of N τ -methylhistidine in the rat. *Br. J. Nutr.*, *38*, 149–151.
- Pietrocola, F., Galluzzi, L., Pedro, Bravo-San., José, M., Madeo, F., & Kroemer, G. (2015). Acetyl coenzyme A: A central metabolite and second messenger. *Cell Metab.*, *21*, 805–821.
- Piroli, G., Manuel, A., Smith, H., McCain, R., Walla, M. and Frizzell, N. (2020) Succination of Dihydrolipoyllysine Succinyltransferase (DLST) Exacerbates Mitochondrial ATP Deficiency in a Mouse Model of Leigh Syndrome, bioRxiv.
- Piroli, G. G., Manuel, A. M., Clapper, A. C., Walla, M. D., Baatz, J. E., Palmiter, R. D., Quintana, A., & Frizzell, N. (2016). Succination is increased on select proteins in the brainstem of the NADH dehydrogenase (ubiquinone) Fe-S protein 4 (Ndufs4) knockout mouse, a model of Leigh syndrome. *Mol. Cell Proteom.*, *15*, 445–461.
- Quintana, A., Kruse, S. E., Kapur, R. P., Sanz, E., & Palmiter, R. D. (2010). Complex I deficiency due to loss of Ndufs4 in the brain results in progressive encephalopathy resembling Leigh syndrome. *PNAS*, *107*, 10996–11001.
- Rahman, J., & Rahman, S. (2018). Mitochondrial medicine in the omics era. *Lancet*, *391*, 2560–2574.
- Rahman, S. (2020). Mitochondrial disease in children. *J. Intern. Med.*, *287*, 609–633.
- Rahman, S., Blok, R., Dahl, H. H., Danks, D., Kirby, D., Chow, C., Christodoulou, J., & Thorburn, D. (1996). Leigh syndrome: Clinical features and biochemical and DNA abnormalities. *Ann. Neurol.*, *39*, 343–351.
- Rodenburg, R. J. (2016). Mitochondrial complex I-linked disease. *Biochim. Biophys. Acta Bioenerg.*, *1857*, 938–945.
- Ruoppolo, M., Caterino, M., Albano, L., Pecce, R., Di Girolamo, M. G., Crisci, D., Costanzo, M., Milella, L., Franconi, F., & Campesi, I. (2018). Targeted metabolomic profiling in rat tissues reveals sex differences. *Sci. Rep.*, *8*, 4663.
- Saggerson, D. (2008). Malonyl-CoA, a key signaling molecule in mammalian cells. *Annu. Rev. Nutr.*, *28*, 253–272.
- Scheiman, J., Luber, J. M., Chavkin, T. A., MacDonald, T., Tung, A., Pham, L.-D., Wibowo, M. C., Wurth, R. C., Punthambaker, S., Tierney, B. T., Yang, Z., Hattab, M. W., Avila-Pacheco, J., Clish, C. B., Lessard, S., Church, G. M., & Kostic, A. D. (2019). Meta-omics analysis of elite athletes identifies a performance-enhancing microbe that functions via lactate metabolism. *Nat. Med.*, *25*, 1104–1109.
- Schiaffino, S., & Reggiani, C. (2011). Fiber types in mammalian skeletal muscles. *Physiol. Rev.*, *91*, 1447–1531.
- Schirris, T. J. J., Rossell, S., de Haas, R., Frambach, S. J. C. M., Hoogstraten, C. A., Renkema, G. H., Beyrath, J. D., Willems, P. H. G. M., Huynen, M. A., Smeitink, J. A. M., Russel, F. G. M., & Notebaart, R. A. (2021). Stimulation of cholesterol biosynthesis in mitochondrial complex I-deficiency lowers reductive stress and improves motor function and survival in mice. *Biochim. Biophys. Acta Mol. Basis Dis.*, *1867*, 166062.
- Schroeder, M. A., Atherton, H. J., Dodd, M. S., Lee, P., Cochlin, L. E., Radda, G. K., Clarke, K., & Tyler, D. J. (2012). The cycling of acetyl-coenzyme A through acetyl carnitine buffers cardiac substrate supply: A hyperpolarized ^{13}C magnetic resonance study. *Circ. Cardiovasc. Imaging*, *5*, 201–209.
- Schwörer, S., Berisa, M., Violante, S., Qin, W., Zhu, J., Hendrickson, R. C., Cross, J. R., & Thompson, C. B. (2020). Proline biosynthesis is a vent for TGF β -induced mitochondrial redox stress. *EMBO J.*, *39*, e103334.
- Schymanski, E. L., Jeon, J., Gulde, R., Fenner, K., Ruff, M., Singer, H. P., & Hollender, J. (2014). Identifying small molecules via high resolution mass spectrometry: Communicating confidence. *Environ. Sci. Technol.*, *48*, 2097–2098.
- Shargill, N. S., Ohshima, K., Bray, G. A., & Chan, T. M. (1984). Muscle protein turnover in the perfused hindquarters of lean and genetically obese-diabetic (db/db) mice. *Diabetes*, *33*, 1160–1164.
- Steele, H. E., Horvath, R., Lyon, J. J., & Chinnery, P. F. (2017). Monitoring clinical progression with mitochondrial disease biomarkers. *Brain*, *140*, 2530–2540.
- Szegedi, S. S., Castro, C. C., Koutmos, M., & Garrow, T. A. (2008). Betaine-homocysteine S-methyltransferase-2 is an S-methylmethionine-homocysteine methyltransferase. *J. Biol. Chem.*, *283*, 8939–8945.
- Teng, Y.-W., Mehendint, M. G., Garrow, T. A., & Zeisel, S. H. (2011). Deletion of betaine-homocysteine S-methyltransferase in mice perturbs choline and 1-carbon metabolism, resulting in fatty liver and hepatocellular carcinomas. *J. Biol. Chem.*, *286*, 36258–36267.
- Terburgh, K., Coetzer, J., Lindeque, J. Z., van der Westhuizen, F. H., & Louw, R. (2021). Aberrant BCAA and glutamate metabolism linked to regional neurodegeneration in a mouse model of Leigh syndrome. *Biochim. Biophys. Acta Mol. Basis Dis.*, *1867*, 166082.
- Terburgh, K., Lindeque, J. Z., Mason, S. W., Van der Westhuizen, F. H., & Louw, R. (2019). Multiplatform metabolomics data from *Ndufs4* $^{-/-}$ skeletal muscles. *Metabolomics Workbench*. <https://doi.org/10.21228/M8GM4Z>
- Terburgh, K., Lindeque, J. Z., van der Westhuizen, F. H., & Louw, R. (2021). Metabolomics of *Ndufs4* KO brain regions. *Metabolomics Workbench*. <https://doi.org/10.21228/M8210V>
- Terburgh, K., Lindeque, J. Z., van der Westhuizen, F. H., & Louw, R. (2021). *Ndufs4* KO mouse urine metabolomics. *Metabolomics Workbench*. <https://doi.org/10.21228/M88M43>
- Terburgh, K., Lindeque, Z., Mason, S., Van der Westhuizen, F., & Louw, R. (2019). Metabolomics of *Ndufs4* $^{-/-}$ skeletal muscle: Adaptive mechanisms converge at the ubiquinone-cycle. *Biochim. Biophys. Acta Mol. Basis Dis.*, *1865*, 98–106.
- van Goudoever, J. B., & Matthews, D. E. (2017). 44 - general concepts of protein metabolism. In: Polin, R.A., Abman, S. H., Rowitch, D. H., Benitz, W. E., & Fox, W. W. (Eds), *Fetal and Neonatal Physiology (Fifth Edition)*, Elsevier. pp. 436-444.e3.
- Vaz, F. M., & Wanders, R. J. (2002). Carnitine biosynthesis in mammals. *Biochem. J.*, *361*, 417–429.
- Venkataraman, A., Rosenbaum, M. A., Werner, J. J., Winans, S. C., & Angenent, L. T. (2014). Metabolite transfer with the fermentation

- product 2,3-butanediol enhances virulence by *Pseudomonas aeruginosa*. *ISME J.*, *8*, 1210–1220.
- Vignoli, A., Tenori, L., Luchinat, C., & Saccenti, E. (2018). Age and sex effects on plasma metabolite association networks in healthy subjects. *J. Proteome Res.*, *17*, 97–107.
- Wassner, S. J., & Li, J. B. (1982). N tau-methylhistidine release: Contributions of rat skeletal muscle, GI tract, and skin. *Am. J. Physiol.*, *243*, E293–E297.
- Wells, A., Barrington, W., Threadgill, D., Dearth, S., Campagna, S., Saxton, A., & Voy, B. (2016). Gene, sex and diet interact to control the tissue metabolome. *FASEB J.*, *30*(127), 2.
- Wilkinson, A. W., Diep, J., Dai, S., Liu, S., Ooi, Y. S., Song, D., Li, T.-M., Horton, J. R., Zhang, X., Liu, C., Trivedi, D. V., Ruppel, K. M., Vilches-Moure, J. G., Casey, K. M., Mak, J., Cowan, T., Elias, J. E., Nagamine, C. M., Spudich, J. A., ... Gozani, O. (2019). SETD3 is an actin histidine methyltransferase that prevents primary dystocia. *Nature*, *565*, 372–376.
- Wu, G., Bazer, F. W., Burghardt, R. C., Johnson, G. A., Kim, S. W., Knabe, D. A., Li, P., Li, X., McKnight, J. R., Satterfield, M. C., & Spencer, T. E. (2011). Proline and hydroxyproline metabolism: Implications for animal and human nutrition. *Amino acids*, *40*, 1053–1063.
- Wu, H., Southam, A. D., Hines, A., & Viant, M. R. (2008). High-throughput tissue extraction protocol for NMR- and MS-based metabolomics. *Anal. Biochem.*, *372*, 204–212.
- Wu, J., & Gao, Y. (2015). Physiological conditions can be reflected in human urine proteome and metabolome. *Expert Rev. Proteom.*, *12*, 623–636.
- Yang, C., Ko, B., Hensley, Christopher T., Jiang, L., Wasti, Ajla T., Kim, J., Suderth, J., Calvaruso, Maria A., Lumata, L., Mitsche, M., Rutter, J., Merritt, Matthew E., & DeBerardinis, Ralph J. (2014). Glutamine oxidation maintains the TCA cycle and cell survival during impaired mitochondrial pyruvate transport. *Mol. Cell*, *56*, 414–424.
- Yang, L., Garcia Canaveras, J. C., Chen, Z., Wang, L., Liang, L., Jang, C., Mayr, J. A., Zhang, Z., Gherguovich, J. M., Zhan, L., Joshi, S., Hu, Z., McReynolds, M. R., Su, X., White, E., Morscher, R. J., & Rabinowitz, J. D. (2020). Serine catabolism feeds NADH when respiration is impaired. *Cell Metab.*, *31*, 809–821.e6.
- Yardeni, T., Tanes, C. E., Bittinger, K., Mattei, L. M., Schaefer, P. M., Singh, L. N., Wu, G. D., Murdock, D. G., & Wallace, D. C. (2019). Host mitochondria influence gut microbiome diversity: A role for ROS. *Sci. Signal.*, *12*, eaaw3159.

Publisher's Note Springer Nature remains neutral with regard to jurisdictional claims in published maps and institutional affiliations.